

East Tennessee State University

Digital Commons @ East Tennessee State University

ETSU Faculty Works

Faculty Works

7-1-2021

Projection Imaging with Ultracold Neutrons

K. Kuk

Fermi National Accelerator Laboratory

C. Cude-Woods

Los Alamos National Laboratory

C. R. Chavez

Fermi National Accelerator Laboratory

J. H. Choi

NC State University

J. Estrada

Fermi National Accelerator Laboratory

See next page for additional authors

Follow this and additional works at: <https://dc.etsu.edu/etsu-works>

Citation Information

Kuk, K.; Cude-Woods, C.; Chavez, C. R.; Choi, J. H.; Estrada, J.; Hoffbauer, M.; Holland, S. E.; Makela, M.; Morris, C. L.; Ramberg, E.; Adamek, E. R.; Bailey, T.; Blatnik, M.; Broussard, L. J.; Brown, M. A.P.; Callahan, N. B.; Clayton, S. M.; and Currie, S.. 2021. Projection Imaging with Ultracold Neutrons. *Nuclear Instruments and Methods in Physics Research, Section A: Accelerators, Spectrometers, Detectors and Associated Equipment*. Vol.1003 <https://doi.org/10.1016/j.nima.2021.165306> ISSN: 0168-9002

This Article is brought to you for free and open access by the Faculty Works at Digital Commons @ East Tennessee State University. It has been accepted for inclusion in ETSU Faculty Works by an authorized administrator of Digital Commons @ East Tennessee State University. For more information, please contact digilib@etsu.edu.

Projection Imaging with Ultracold Neutrons

Copyright Statement

© 2021 The Author(s). Published by Elsevier B.V. This is an open access article under the CC BY-NC-ND license (<http://creativecommons.org/licenses/by-nc-nd/4.0/>).

Creative Commons License



This work is licensed under a [Creative Commons Attribution-NonCommercial-No Derivative Works 4.0 International License](https://creativecommons.org/licenses/by-nc-nd/4.0/).

Creator(s)

K. Kuk, C. Cude-Woods, C. R. Chavez, J. H. Choi, J. Estrada, M. Hoffbauer, S. E. Holland, M. Makela, C. L. Morris, E. Ramberg, E. R. Adamek, T. Bailey, M. Blatnik, L. J. Broussard, M. A.P. Brown, N. B. Callahan, S. M. Clayton, and S. Currie



Projection imaging with ultracold neutrons

K. Kuk^a, C. Cude-Woods^{b,c}, C.R. Chavez^a, J.H. Choi^c, J. Estrada^{a,*}, M. Hoffbauer^b, S.E. Holland^d, M. Makela^b, C.L. Morris^b, E. Ramberg^a, E.R. Adamek^e, T. Bailey^c, M. Blatnik^f, L.J. Broussard^b, M.A.-P. Brown^g, N.B. Callahan^h, S.M. Clayton^b, S. Currie^b, B.W. Filippone^f, E.M. Fries^f, P. Geltenbortⁱ, F. Gonzalez^h, M.T. Hassan^b, L. Hayen^c, K.P. Hickerson^f, A.T. Holley^j, T.M. Ito^b, C.-Y. Liu^h, P. Merkel^a, R. Musedinovic^c, C. O'Shaughnessy^b, R.W. Pattie Jr.^k, B. Plaster^g, D.J. Salvat^h, A. Saunders^b, E.I. Sharapov^l, X. Sun^f, Z. Tang^b, W. Wei^f, J.W. Wexler^c, A.R. Young^c, Zhehui Wang^{b,*}

^a Fermi National Accelerator Laboratory, Batavia, IL 60510, USA

^b Los Alamos National Laboratory, Los Alamos, NM 87545, USA

^c North Carolina State University, Raleigh, NC 27695, USA

^d Lawrence Berkeley National Laboratory, Berkeley, CA 94720, USA

^e The University of Tennessee, Knoxville, TN 37996, USA

^f California Institute of Technology, Pasadena, CA 91125, USA

^g University of Kentucky, Lexington, KY 40506, USA

^h Indiana University, Bloomington, IN 47405, USA

ⁱ Institut Laue Langevin, 38042 Grenoble, France

^j Tennessee Technological University, Cookeville, TN 38505, USA

^k East Tennessee State University, Johnson City, TN 37614, USA

^l Joint Institute for Nuclear Research, 141980, Dubna, Russia

ARTICLE INFO

Keywords:

Ultracold neutrons

Direct detection

¹⁰B nanometer thin film

Neutron detection efficiency

Low background

Projection imaging

ABSTRACT

Ultracold neutron (UCN) projection imaging is demonstrated using a boron-coated back-illuminated CCD camera and the Los Alamos UCN source. Each neutron is recorded through the capture reactions with ¹⁰B. By direct detection at least one of the byproducts α , ⁷Li and γ (electron recoils) derived from the neutron capture and reduction of thermal noise of the scientific CCD camera, a signal-to-noise improvement on the order of 10⁴ over the indirect detection has been achieved. Sub-pixel position resolution of a few microns is confirmed for individual UCN events. Projection imaging of test objects shows a spatial resolution less than 100 μm by an integrated UCN flux one the order of 10⁶ cm^{-2} . The bCCD can be used to build UCN detectors with an area on the order of 1 m^2 . The combination of micrometer scale spatial resolution, low readout noise of a few electrons, and large area makes bCCD suitable for quantum science of UCN.

1. Introduction

With a kinetic energy less than 400 neV, ultracold neutrons (UCN) are the coldest free neutrons known in the laboratory and the universe. UCN have been used to examine fundamental interactions in nature through precise measurement of the neutron lifetime [1,2], determine properties of neutron beta decay [3], and search for the neutron electric dipole moment [4–6]. There is growing interest in using position-sensitive measurements of UCN to study fundamental quantum states of UCN. For example, quantum states of UCN in the Earth's gravity field have been reported experimentally in 2002 [7]. The de Broglie wavelength of UCN (λ_n) is

$$\lambda_n = \frac{904.5}{\sqrt{E_n}} = \frac{395.6}{v_n}, \quad (1)$$

where λ_n is in nm, the kinetic energy of the neutron (E_n) in neV and the velocity of the neutron (v_n) in m/s. For a UCN with a kinetic energy of 82 neV or a velocity of 3.96 m/s, $\lambda_n = 100$ nm. Precise measurements of quantum states of UCN can be used in dark energy and dark matter search [8–10]. Gravitationally bound UCN might also be used to test Newton's inverse square law of gravity at short distances from 0.1–100 μm [11–13]. Depending on the reflecting boundary and UCN wavelength, gravity quantum states measurements require a spatial resolution less than 10 μm , and 1 μm or less is highly desired.

* Corresponding authors.

E-mail addresses: estrada@fnal.gov (J. Estrada), zwang@lanl.gov (Z. Wang).

Position-sensitive measurements of UCN based on ZnS:Ag scintillators or indirect detection were reported previously [14–16]. Isotopically purified ^{10}B thin films were used to capture UCN through the reactions: $^{10}\text{B}(n, \alpha)^7\text{Li}$ (6%) and $^{10}\text{B}(n, \alpha)^7\text{Li}$ (94%). For UCN at 3.96 m/s, the $1/e$ -absorption (36.8% attenuation) thickness of ^{10}B film is $\lambda_a = \tau_0 v_n = 35.6$ nm. The average absorption time $\tau_0 = 9.0$ ns in ^{10}B (at solid density 2.2 g/cm³) is independent of neutron velocity. Position resolution was limited either by the size of the photomultipliers [14,16] or by the light yield and optics for the intensified imaging camera [15]. Here we describe a direct detection scheme when a ^{10}B thin film up to 100 nm is deposited on the backside of a scientific CCD camera [17,18]. Charge carriers (electron-hole pairs) are created when the α , ^7Li and γ from the neutron capture reactions are stopped or scattered in the thick silicon layer (~ 300 μm). The low energy threshold (3.6 eV per pair) for charge production in silicon, CCD cooling, and the elimination of optics have led to a signal-to-noise improvement on the order of 10^4 over the indirect detection scheme based on ZnS:Ag scintillator. In addition to the fulfillment of the initial requirements for applications in quantum physics and quantum information of UCN, we have also obtained results of UCN projection imaging using several test objects.

Below we first describe the boron-coated CCD (bCCD) detector and the experimental setup. Next, we show UCN projection imaging of several test objects, and the analysis of detector energy and position resolution. We conclude that bCCD would find applications in both fundamental science of UCN and projection imaging of more complex samples with a spatial resolution below 100 μm .

2. bCCD and the UCN detection principle

The working principle of the bCCD detector is illustrated in Fig. 1. The scientific CCDs used in this work are scientific-grade sensors similar to those in the Dark Energy Camera (DECam) wide field imager [18], built by the Lawrence Berkeley National Laboratory (LBNL) [17]. The CCD sensors have been extensively characterized at Fermilab for the DECam project [19]. The DECam CCDs are 250 μm thick, fully depleted, back-illuminated devices fabricated on high-resistivity silicon. Each CCD sensor used for this study has 8 million pixels ($2\text{k} \times 4\text{k}$) with dimensions 15 $\mu\text{m} \times 15$ μm . Fig. 1 shows the 3-phase, p-channel CCD design. The 10 k Ω -cm resistivity, allows for a fully depleted operation at bias voltages of 25 V. The field extends essentially all the way to the backside contact, depleting the entire volume of the CCD substrate. The CCD readout noise has been found to be 7.6 ADU = 8.5 e^- for a pixel time of 4 μs per pixel with thermal electric cooling.

When an ionizing particle such as α , ^7Li or γ -ray penetrates the detector, it creates electron-hole (e-h) pairs. Under the influence of the electric field, the holes produced near the back surface (α and ^7Li) will travel the full thickness of the device to reach the potential well near the gates. Particle identification for this detector has been discussed in a previous work [20] with special attention paid to identifying heavily ionizing α particles, as discussed in Ref. [21]. The α particles, such as those expected from the neutron capture reactions $^{10}\text{B}(n, \alpha)^7\text{Li}$ (6%) and $^{10}\text{B}(n, \alpha)^7\text{Li}$ (94%) are easily identified in CCD images due to the plasma effect. These CCDs have been used previously for thermal neutron detection using a 1 μm thick boron film in a ceramic substrate that was positioned close to the CCD, as discussed in Ref. [22]. For this work, the back side of the CCD was directly coated with ^{10}B to less than 100 nm thick, using the same electron-beam evaporation method described previously [14]. We show below that this boron-coated CCD (bCCD) sensor becomes an excellent choice for detecting UCN with less than 10- μm (sub-pixel) position resolution, good energy resolution (for the by-products from the UCN-capture) and high efficiency.

The performance of the bCCD was tested at the Los Alamos UCN facility [23]. The Los Alamos UCN source uses a combination of beryllium, graphite moderators at ambient temperature, and solid deuterium at 5 K, to cool spallation MeV neutrons by 13 orders of magnitude

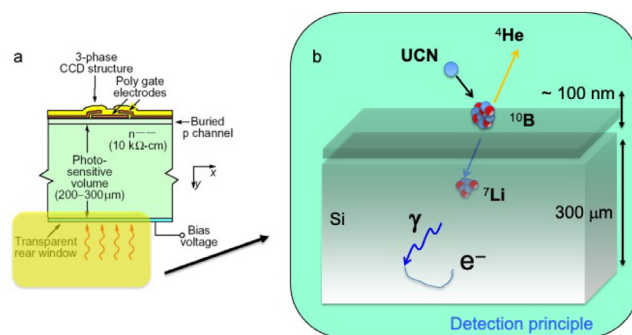


Fig. 1. (a) The pixel cross section of a fully-depleted back-illuminated CCD developed at Lawrence Berkeley Laboratory [17]. (b) The CCD backside is coated with a ^{10}B top layer up to 100 nm thick, using the electron-evaporation deposition process described in [14]. At least one of the charged particles α or ^7Li generated from the neutron capture slows down and stops in the fully depleted layer and creates e-h pairs. The companion γ -ray (480 keV) photon is emitted isotropically into the 4π solid angle with respect to the UCN capture location. Up to 50% of the γ -rays are intercepted by the silicon layer and generate a corresponding Compton electron (e^-), which then produces e-h pairs as signatures for the γ photons.

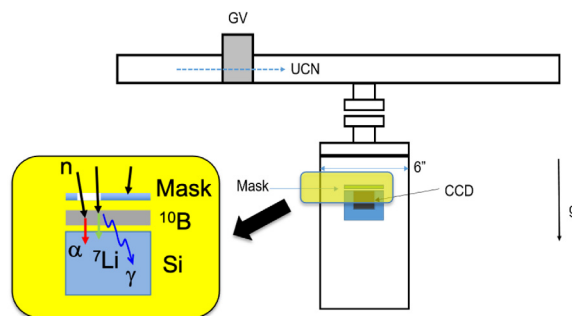


Fig. 2. The schematic of the experimental setup. The UCN flux to the detector chamber is controlled by a gate valve (GV). The CCD detector faces up. Experiments are conducted both with and without a mask on the top of the CCD back side. The readout electronics (outside the vacuum chamber), the vacuum interface for the bCCD data cables, and on-board electronics (inside the vacuum chamber) are not shown.

to mK temperatures. The resulting UCN move at speeds of only a few meters per second, and can be completely confined by magnetic fields and/or material walls such as a stainless steel tube. The bCCD was installed inside a stainless steel vacuum vessel (the base vacuum on the order of 10^{-6} Torr for the data shown here), and cooled to 140 K to suppress dark current. This vessel was then connected to the UCN source through stainless steel neutron guides as shown in Fig. 2. The sensor was positioned with the borated surface facing up, and directly exposed to the UCN flux when the gate valve is open.

3. Results and discussion

The spatial resolution of the UCN projection imaging was characterized using two different masks. The first mask was a 3D printed ‘UCN’ letter pattern (transparent to UCN) on a rectangular thermoplastic material. The mask target was placed at ~ 3 mm away from the borated surface of the bCCD, and covered completely the imaging sensor. The detector was then exposed to UCN during which the neutron-capture events were recorded. The pattern of the mask was reproduced quite well by summing the recorded events in the CCD over a certain period of time, as shown in Fig. 3. This initial test qualitatively demonstrates the projection imaging capability of the bCCD in conjunction with the Los Alamos UCN source. The data shown also clearly demonstrate the particle identification capability of the sensor, similar to previous results [21]. Heavily ionizing particles (α and Li ions) and Compton

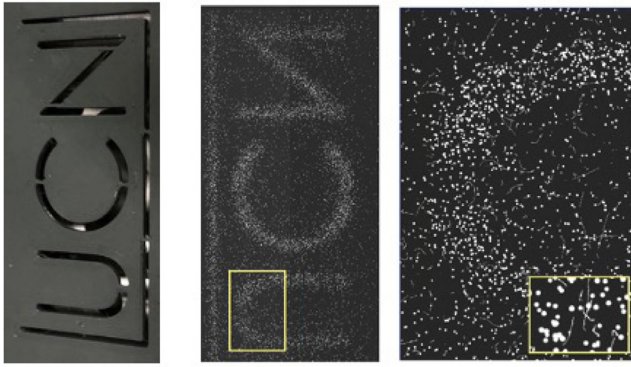


Fig. 3. (Left) A 3D printed rectangular mask using thermoplastic material. This mask covered the full size of the detector (6 cm × 3 cm). The mask was positioned about 3 mm above the borated surface of the bCCD. (Center) A raw bCCD image showing the transmission flux of UCN through the mask. (Right) Zoom into the yellow box at the center panel, showing the hits from the different particles and different energies from the neutron capture reactions. Inset shows a zoom into an even smaller region of the image.

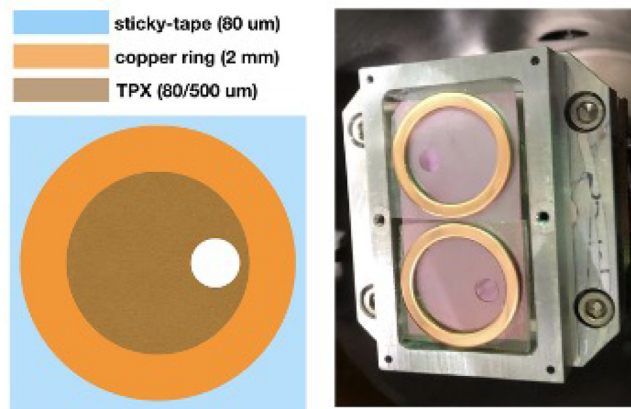


Fig. 4. (Left) Schematic of the three layer mask used in front of the bCCD. Two versions of this mask were used, with different thickness of the kapton tape (80 μm and 500 μm). (Right) Photograph of the two masks directly mounted in contact with the borated surface of the bCCD.

scattering from γ s produced are distinguishable from their different pixel patterns derived from the individual ion or electron tracks.

A refined measurement of the position resolution was performed with a second mask, when the distance between the mask and the boron-coated surface is reduced to less than 100 μm (the size of a human hair). This mask was built with 3 layers: (a) copper ring (2 mm diameter), (b) double-sided sticky tape 80 μm thick, and (c) Polymethylpentene film (trademark TPX) which came in two different thicknesses of 0.5 mm and 80 μm. These layers were arranged as shown in Fig. 4. A circular hole was punched through the complete assembly. In this case the mask was brought into direct contact with the borated surface of the bCCD. Two similar masks were built and installed next to each other to cover the full imaging detector as shown in Fig. 4. The resulting hit map (about 5 min of UCN flux) is shown in Fig. 5. Here, only the hits consistent with the circular charge clusters produced by heavily ionizing particles were selected. All the tracks from the Compton electrons have been removed.

The smaller circle in the lower left in Fig. 5 is used for the estimation of the position resolution. The centroid for the circle is calculated, and the distribution of hits per unit area is shown for that circle in Fig. 6. This distribution is fitted to the convolution of a gaussian resolution with a step function, and the results of the fit are shown in Fig. 6, indicating a gaussian resolution of 13 pixels (195 μm). It should be

Table 1

Maximum ion ranges (R') of the charged products and their relative detection probabilities (w') from the $^{10}\text{B}(n, \alpha)^7\text{Li}$ neutron capture process in ^{10}B solid films and Si. A possible dead layer may exist in between the ^{10}B layer and fully charge depleted region of Si sensor, which could reduce the actual range and energy in the Si sensor.

Ion (w')	Energy (E'_0 , MeV)	Range in ^{10}B (R' , μm)	Range in Si (R' , μm)
α (47%)	1.47	3.5	5.1
α (3%)	1.78	4.4	6.4
^7Li (47%)	0.84	1.8	2.5
^7Li (3%)	1.02	2.1	2.8

noted that the mask was not cut with micron level precision for this initial experiment, and part of this resolution can be attributed to the mask fabrication. To demonstrate the issue of the mask imperfection, a new fit was performed using only the upper right quadrant of the circle giving a resolution of 4 pixels (60 μm).

The position resolution in Fig. 6 is likely limited by imperfections on the mask, and not by the intrinsic position resolution of the detector. The hits produced by heavily ionizing particles are extended over many pixels, and their centroid can be determined with sub-pixel precision. To demonstrate this we fit the charge distribution produced by a single highly ionizing hit reconstructed on the bCCD image. As shown in Fig. 7, the centroid of each hit can be determined with an uncertainty significantly smaller than a pixel. The fit shown in Fig. 7 has an uncertainty of 0.1 pixel (1.5 μm). The intrinsic resolution of the detector will also be limited by the range of the α particles inside the silicon [22]. Their range has been calculated using the Stopping and Range of Ions in Matter (SRIM) code and is expected to be no more than 6.4 μm as shown in Table 1, and therefore significantly less than the fully depleted Si layer thickness of 250 μm. The energy loss in the ^{10}B layer and the dead layer on the surface of the silicon active region will reduce the actual energy deposition and stopping ranges of the ions in silicon.

Since the ion ranges in silicon are many times the ^{10}B film thickness $T_0 < 100$ nm, the charged particle energy losses in the ^{10}B are small, except for the ions that move at large angles with respect to the surface normal. The range loss due to ^{10}B and the dead layer is most significant for the 0.84 MeV ^7Li ions. The full ion stopping in ^{10}B only occurs when the angle is greater than $\theta_c = \cos^{-1}(T_0/R')$, or about 87.4 degrees for $T_0 = 80$ nm.

The CCD detector was calibrated using an ^{55}Fe radioactive source producing mainly 5.9 keV X-rays [19]. This calibration was then used to measure the energy of the events consistent with a heavily ionizing particle resulting from the neutron capture. The energy spectrum for the heavily ionization events observed during the UCN exposure is shown in Fig. 8. The position of the energy peak for the α is properly reconstructed, while the ^7Li is shifted to about 0.7 MeV. A more detailed study of the reconstruction and dead layers will have to be performed to understand this down-shift quantitatively. However, it is clear that it is possible to separate both types of events, allowing possible achievable position resolution for single neutron capture events to be below the upper limit of 6.4 μm.

The observed α and ^7Li peaks can be fitted by a skewed Gaussian function [14],

$$f(x) = 2c_1 \phi(x') \Phi(\alpha_s x') + c_0, \quad (2)$$

with

$$x' = \frac{x - x_0}{\sigma}, \quad (3)$$

$$\phi(x) = \frac{1}{\sqrt{2\pi}} e^{-x^2/2}, \quad (4)$$

and

$$\Phi(x) = \frac{1}{2} \left[1 + \operatorname{erf}\left(\frac{x}{\sqrt{2}}\right) \right]. \quad (5)$$

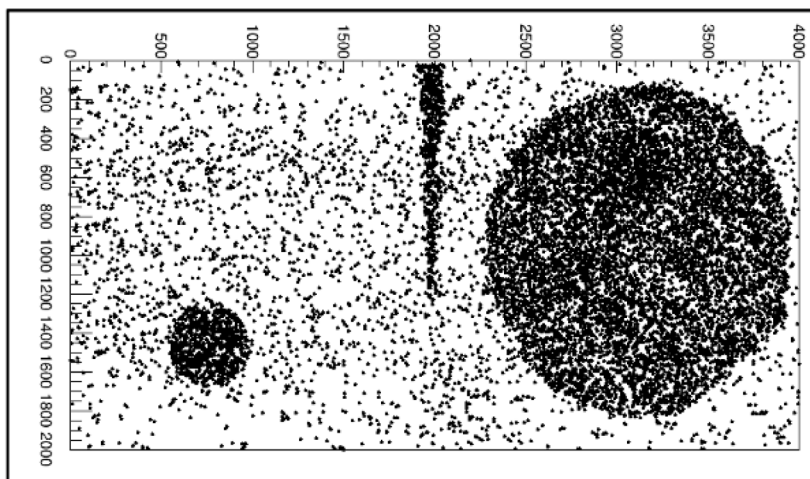


Fig. 5. Hit map for the observed heavily ionizing particles for the setup discussed in Fig. 4 and a UCN exposure time of 5 min. The circles produced by the different layers of the mask are clearly reconstructed. The hit map also shows the triangular gap between the two masks.

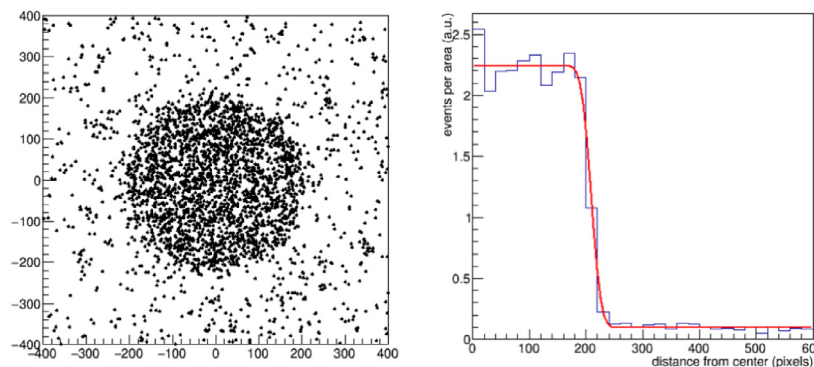


Fig. 6. (Left) Hit map for heavily ionizing particles reconstructed on the bCCD image for the setup in Fig. 4. This is a subsection of the hit map shown in Fig. 5, with the horizontal and vertical scale centered at the circular feature in the bottom right of Fig. 5. (Right) The number of hits per unit area is shown as a function of distance from the center of the circle. The red curve shows the fit to a step function with a gaussian position resolution as discussed in the text. (For interpretation of the references to color in this figure legend, the reader is referred to the web version of this article.)

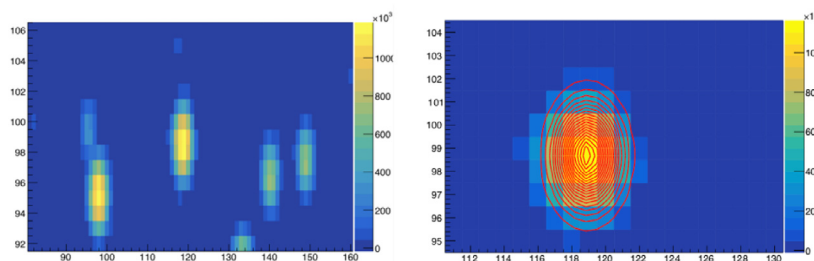


Fig. 7. (Left) A small region of reconstructed bCCD image with 5 heavily ionizing hits. Both axes are in pixels, and the color scale is in digital units corresponding to 40 counts/electron. (Right) Zoom in the region around column 120. The red contours correspond to a 2D gaussian fit to the hit, demonstrating the determination of the centroid with a sub-pixel resolution. (For interpretation of the references to color in this figure legend, the reader is referred to the web version of this article.)

The fitting parameters for 0.84 MeV ${}^7\text{Li}$ are $x_0 = 700$, $\sigma = 60.5$. The model may be further used to guide us to improve the position resolution.

4. Conclusions

In summary, UCN projection imaging is demonstrated using a back illuminated CCD at the Los Alamos UCN facility. A thin layer (<100 nm) of ${}^{10}\text{B}$ was directly deposited on the CCD back surface. We show that it is possible to separate the products of the neutron capture (α and ${}^7\text{Li}$) and the Compton events produced from gamma radiation. A position resolution of $60\ \mu\text{m}$ has been demonstrated using a mask installed

directly on top of the bCCD. This is still far from the ultimate position resolution estimated for this technique. The interpretation of the TPX mask edge is complicated by the penumbra produced because of UCN absorption in the edge of the plastic above the surface, which is thick compared to the expected resolution of the detector. This effect can be mitigated in future tests by using a reflective rather than an absorptive material in contact with the CCD.

The bCCD detector also provides a new technique for the measurement of individual UCN with high position and energy resolution. Several ongoing and planned experiments could benefit from the performance shown here, such as real-time detector in studying UCN quantum states in the Earth's gravitational field. Other possible

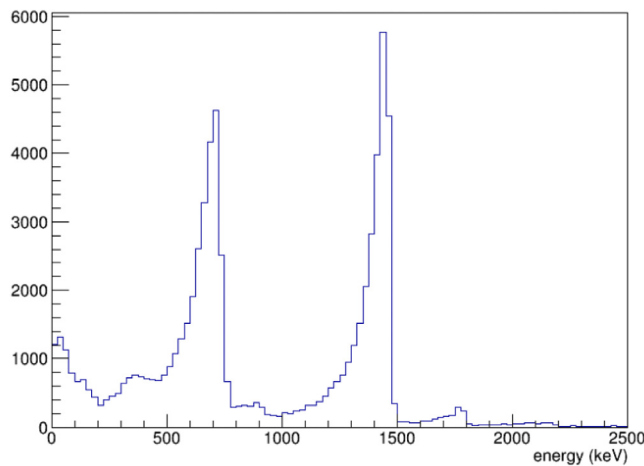


Fig. 8. UCN capture spectrum as measured by the calibrated bCCD (expected: $\alpha = 1.47$ MeV, $\text{Li} = 0.84$ MeV).

applications include UCN microscopy and reflectometry for material science [15]. Opportunities to examine the quantum properties of UCN, building on demonstrations of quantum physics under gravity, have also been recognized by the community report [24]. Current UCN experiments with position measurements have been performed and planned as a probe of dark energy models [9,25]. The greatly enhanced UCN position resolution from the device discussed here could enhance the capability of these experiments through for example, real-time measurements. The high resolution in position may be converted into high energy resolution using a proper experimental set-up.

CRedit authorship contribution statement

K. Kuk: Performed the experiment using B-10 coated CCD, Designed and made the masks. **C. Cude-Woods:** Performed the experiment using B-10 coated CCD, Designed and made the masks, UCN facility operation, planning, and/or UCN source support and/or inputs to the experimental execution. **C.R. Chavez:** Performed the experiment using B-10 coated CCD. **J.H. Choi:** Performed the experiment using B-10 coated CCD, UCN facility operation, planning, and/or UCN source support and/or inputs to the experimental execution. **J. Estrada:** CCD detector design and/or hardware, Led the data analysis with inputs from the Fermilab team and LANL team, Led the manuscript writing with inputs from all the coauthors. **M. Hoffbauer:** CCD B-10 coating plan and performed the B-10 coating. **S.E. Holland:** CCD detector design and/or hardware. **M. Makela:** Performed the experiment using B-10 coated CCD, Designed and made the masks, UCN facility operation, planning, and/or UCN source support and/or inputs to the experimental execution. **C.L. Morris:** Performed the experiment using B-10 coated CCD, Designed and made the masks, UCN facility operation, planning, and/or UCN source support and/or inputs to the experimental execution. **E. Ramberg:** CCD detector design and/or hardware. **E.R. Adamek:** UCN facility operation, planning, and/or UCN source support and/or inputs to the experimental execution. **T. Bailey:** UCN facility operation, planning, and/or UCN source support and/or inputs to the experimental execution. **M. Blatnik:** UCN facility operation, planning, and/or UCN source support and/or inputs to the experimental execution. **L.J. Broussard:** UCN facility operation, planning, and/or UCN source support and/or inputs to the experimental execution. **M.A.-P. Brown:** UCN facility operation, planning, and/or UCN source support and/or inputs to the experimental execution. **N.B. Callahan:** UCN facility operation, planning, and/or UCN source support and/or inputs to the experimental execution. **S.M. Clayton:** UCN facility operation, planning, and/or UCN source support and/or inputs

to the experimental execution. **S. Currie:** UCN facility operation, planning, and/or UCN source support and/or inputs to the experimental execution. **B.W. Filippone:** UCN facility operation, planning, and/or UCN source support and/or inputs to the experimental execution. **E.M. Fries:** UCN facility operation, planning, and/or UCN source support and/or inputs to the experimental execution. **P. Geltenbort:** UCN facility operation, planning, and/or UCN source support and/or inputs to the experimental execution. **F. Gonzalez:** UCN facility operation, planning, and/or UCN source support and/or inputs to the experimental execution. **M.T. Hassan:** UCN facility operation, planning, and/or UCN source support and/or inputs to the experimental execution. **L. Hayen:** UCN facility operation, planning, and/or UCN source support and/or inputs to the experimental execution. **K.P. Hickerson:** UCN facility operation, planning, and/or UCN source support and/or inputs to the experimental execution. **A.T. Holley:** UCN facility operation, planning, and/or UCN source support and/or inputs to the experimental execution. **T.M. Ito:** UCN facility operation, planning, and/or UCN source support and/or inputs to the experimental execution. **C.-Y. Liu:** UCN facility operation, planning, and/or UCN source support and/or inputs to the experimental execution. **P. Merkel:** CCD detector design and/or hardware. **R. Musedinovic:** UCN facility operation, planning, and/or UCN source support and/or inputs to the experimental execution. **C. O'Shaughnessy:** UCN facility operation, planning, and/or UCN source support and/or inputs to the experimental execution. **R.W. Pattie Jr.:** UCN facility operation, planning, and/or UCN source support and/or inputs to the experimental execution. **B. Plaster:** UCN facility operation, planning, and/or UCN source support and/or inputs to the experimental execution. **D.J. Salvat:** UCN facility operation, planning, and/or UCN source support and/or inputs to the experimental execution. **A. Saunders:** UCN facility operation, planning, and/or UCN source support and/or inputs to the experimental execution. **E.I. Sharapov:** UCN facility operation, planning, and/or UCN source support and/or inputs to the experimental execution. **X. Sun:** UCN facility operation, planning, and/or UCN source support and/or inputs to the experimental execution. **Z. Tang:** UCN facility operation, planning, and/or UCN source support and/or inputs to the experimental execution. **W. Wei:** UCN facility operation, planning, and/or UCN source support and/or inputs to the experimental execution. **J.W. Wexler:** UCN facility operation, planning, and/or UCN source support and/or inputs to the experimental execution. **A.R. Young:** UCN facility operation, planning, and/or UCN source support and/or inputs to the experimental execution. **Zhehui Wang:** Performed the experiment using B-10 coated CCD, CCD detector design and/or hardware, CCD B-10 coating plan and performed the B-10 coating, Led the manuscript writing with inputs from all the coauthors, Initiated the work with feedbacks and refinement of the plans from all the coauthors.

Declaration of competing interest

The authors declare that they have no known competing financial interests or personal relationships that could have appeared to influence the work reported in this paper.

Acknowledgments

This work was funded by the LDRD program of Los Alamos National Laboratory, USA. The CCD development work was supported in part by the Director, Office of Science, of the U.S. Department of Energy under Contract No. DE-AC02-05CH11231. NCSU is supported by National Science Foundation, USA 1914133 and DOE, USA grant DE-FG02-ER41042.

References

- [1] A.P. Serebrov, E.A. Kolomensky, A.K. Fomin, I.A. Krasnoschekova, A.V. Vassiljev, D.M. Prudnikov, I.V. Shoka, A.V. Checkkin, M.E. Chaikovskiy, V.E. Varlamov, S.N. Ivanov, A.N. Pirozhkov, P. Geltenbort, O. Zimmer, T. Jenke, M. Van der Grinten, M. Tucker, *Phys. Rev. C* 97 (2018) 055503.
- [2] R.W. Pattie, N.B. Callahan, C. Cude-Woods, E.R. Adamek, L.J. Broussard, S.M. Clayton, S.A. Currie, E.B. Dees, X. Ding, E.M. Engel, D.E. Fellers, W. Fox, P. Geltenbort, K.P. Hickerson, M.A. Hoffbauer, A.T. Holley, A. Komives, C.-Y. Liu, S.W.T. MacDonald, M. Makela, C.L. Morris, J.D. Ortiz, J. Ramsey, D.J. Salvat, A. Saunders, S.J. Seestrom, E.I. Sharapov, S.K. Sjuue, Z. Tang, J. Vanderwerp, B. Vogelaar, P.L. Walstrom, Z. Wang, W. Wei, H.L. Weaver, J.W. Wexler, T.L. Womack, A.R. Young, B.A. Zeck, *Science* 360 (2018) 627.
- [3] M.A.-P. Brown, E.B. Dees, E. Adamek, B. Allgeier, M. Blatnik, T.J. Bowles, L.J. Broussard, R. Carr, S. Clayton, C. Cude-Woods, S. Currie, X. Ding, B.W. Filippone, A. García, P. Geltenbort, R. Hasan, K.P. Hickerson, J. Hoagland, R. Hong, G.E. Hogan, A.T. Holley, T.M. Ito, A. Knecht, C.-Y. Liu, J. Liu, M. Makela, J.W. Martin, D. Melconian, M.P. Mendenhall, S.D. Moore, C.L. Morris, S. Nepal, N. Nouri, R.W. Pattie Jr, A. Pérez Galván, I.L.D.G. Phillips, R. Picker, M.L. Pitt, B. Plaster, J.C. Ramsey, R. Rios, D.J. Salvat, A. Saunders, D.W. Schmidt, R.K. Schulze, S.J. Seestrom, E.I. Sharapov, A. Sprow, Z. Tang, W. Wei, J. Wexler, T.L. Womack, A.R. Young, B.A. Zeck, *Nucl. Instrum. Methods A* 798 (2015) 30.
- [4] J.M. Pendlebury, S. Afach, N.J. Ayres, C.A. Baker, G. Ban, G. Bison, K. Bodek, M. Burghoff, P. Geltenbort, K. Green, W.C. Griffith, M. van der Grinten, Z.D. Gruić, P.G. Harris, V. Hélaine, P. Iaydjiev, S.N. Ivanov, M. Kasprzak, Y. Kermaidic, K. Kirch, H.-C. Koch, S. Komposch, A. Kozela, J. Krempel, B. Lauss, T. Lefort, Y. Lemièrre, D.J.R. May, M. Musgrave, O. Naviliat-Cuncic, F.M. Piegsa, G. Pignol, P.N. Prashanth, G. Quémener, M. Rawlik, D. Rebreyend, J.D. Richardson, D. Ries, S. Roccia, D. Rozpedzik, A. Schnabel, P. Schmidt-Wellenburg, N. Severijns, D. Shiers, J.A. Thorne, A. Weis, O.J. Winston, E. Wursten, J. Zejma, G. Zsigmond, *Phys. Rev. D* 92 (2015) 092003.
- [5] B.W. Filippone, arXiv:1810.03718, 2018.
- [6] C. Abel, S. Afach, N.J. Ayres, C.A. Baker, G. Ban, G. Bison, K. Bodek, V. Bondar, M. Burghoff, E. Chanel, Z. Chowdhuri, P.-J. Chiu, B. Clement, C.B. Crawford, M. Daum, S. Emmenegger, L. Ferraris-Bouchez, M. Fertl, P. Flaux, B. Franke, A. Fratangelo, P. Geltenbort, K. Green, W.C. Griffith, M. van der Grinten, Z.D. Gruić, P.G. Harris, L. Hayen, W. Heil, R. Henneck, V. Hélaine, N. Hild, Z. Hodge, M. Horras, P. Iaydjiev, S.N. Ivanov, M. Kasprzak, Y. Kermaidic, K. Kirch, A. Knecht, P. Knowles, H.-C. Koch, P.A. Koss, S. Komposch, A. Kozela, A. Kraft, J. Krempel, M. Kuźniak, B. Lauss, T. Lefort, Y. Lemièrre, A. Leredde, P. Mohanmurthy, A. Mtchedlishvili, M. Musgrave, O. Naviliat-Cuncic, D. Pais, F.M. Piegsa, E. Pierre, G. Pignol, C. Plonka-Spehr, P.N. Prashanth, G. Quémener, M. Rawlik, D. Rebreyend, I. Rienäcker, D. Ries, S. Roccia, G. Rogel, D. Rozpedzik, A. Schnabel, P. Schmidt-Wellenburg, N. Severijns, D. Shiers, R. Tavakoli Dinani, J.A. Thorne, R. Viro, J. Voigt, A. Weis, E. Wursten, G. Wyszynski, J. Zejma, J. Zenner, G. Zsigmond, *Phys. Rev. Lett.* 124 (2020) 081803.
- [7] V.V. Nesvizhevsky, H.G. Börner, A.K. Petukhov, H. Abele, S. Baefßler, F.J. Ruef, T. Stöferle, A. Westphal, A.M. Gagarski, G.A. Petrov, A.V. Strelkov, *Nature* 415 (2002) 297.
- [8] T. Jenke, G. Cronenberg, J. Burgdörfer, L.A. Chizhova, P. Geltenbort, A.N. Ivanov, T. Lauer, T. Lins, S. Rotter, H. Saul, U. Schmidt, H. Abele, *Phys. Rev. Lett.* 112 (2014) 151105.
- [9] G. Pignol, *Internat. J. Modern Phys. A* 30 (2015) 1530048.
- [10] Xuan. Sun, E. Adamek, B. Allgeier, M. Blatnik, T.J. Bowles, L.J. Broussard, M.A.-P. Brown, R. Carr, S. Clayton, C. Cude-Woods, S. Currie, E.B. Dees, X. Ding, B.W. Filippone, A. García, P. Geltenbort, S. Hasan, K.P. Hickerson, J. Hoagland, R. Hong, G.E. Hogan, A.T. Holley, T.M. Ito, A. Knecht, C.-Y. Liu, J. Liu, M. Makela, R. Mammei, J.W. Martin, D. Melconian, M.P. Mendenhall, S.D. Moore, C.L. Morris, S. Nepal, N. Nouri, R.W. Pattie Jr, A. Pérez Galván, I.L.D.G. Phillips, R. Picker, M.L. Pitt, B. Plaster, J.C. Ramsey, R. Rios, D.J. Salvat, A. Saunders, W. Sondheim, S. Sjuue, S. Slutsky, C. Swank, G. Swift, E. Tatar, R.B. Vogelaar, B. VornDick, Z. Wang, W. Wei, J. Wexler, T. Womack, C. Wrede, A.R. Young, B.A. Zeck, UCNA Collaboration, *Phys. Rev. C* 97 (2018) 052501.
- [11] J.S. Nico, W.M. Snow, *Ann. Rev. Nucl. Part. Sci.* 55 (2005) 27–69.
- [12] H. Abele, *Prog. Part. Nucl. Phys.* 60 (1) (2008).
- [13] D. Dubbers, M.G. Schmidt, *Rev. Modern Phys.* 83 (2011) 1111.
- [14] Z. Wang, M.A. Hoffbauer, C.L. Morris, N.B. Callahan, E.R. Adamek, J.D. Bacon, M. Blatnik, A.E. Brandt, L.J. Broussard, S.M. Clayton, C. Cude-Woods, S. Currie, E.B. Dees, X. Ding, J. Gao, F.E. Gray, K.P. Hickerson, A.T. Holley, T.M. Ito, C.-Y. Liu, M. Makela, J.C. Ramsey, R.W. Pattie Jr, D.J. Salvat, A. Saunders, D.W. Schmidt, R.K. Schulze, S.J. Seestrom, E.I. Sharapov, A. Sprow, Z. Tang, W. Wei, J. Wexler, T.L. Womack, A.R. Young, B.A. Zeck, *Nucl. Instrum. Methods A* 798 (2015) 30.
- [15] W. Wei, L.J. Broussard, M.A. Hoffbauer, M. Makela, C.L. Morris, Z. Tang, E. Adamek, N.B. Callahan, S.M. Clayton, C. Cude-Woods, S. Currie, E.B. Dees, X. Ding, P. Geltenbort, K.P. Hickerson, A.T. Holley, T.M. Ito, K.K. Leung, C.-Y. Liu, D.J. Morley, J.D. Ortiz, R.W. Pattie Jr, J.C. Ramsey, A. Saunders, S.J. Seestrom, E.I. Sharapov, S.K. Sjuue, J. Wexler, T.L. Womack, A.R. Young, B.A. Zeck, Z. Wang,
- [16] C.L. Morris, E.R. Adamek, L.J. Broussard, N.B. Callahan, S.M. Clayton, C. Cude-Woods, S.A. Currie, X. Ding, W. Fox, K.P. Hickerson, M.A. Hoffbauer, A.T. Holley, A. Komives, C.-Y. Liu, M. Makela, R.W. Pattie Jr, J. Ramsey, D.J. Salvat, A. Saunders, S.J. Seestrom, E.I. Sharapov, S.K. Sjuue, Z. Tang, J. Vanderwerp, B. Vogelaar, P.L. Walstrom, Z. Wang, W. Wei, J.W. Wexler, T.L. Womack, A.R. Young, B.A. Zeck, *Rev. Sci. Instrum.* 88 (5) (2017) 053508.
- [17] S.E. Holland, D.E. Groom, N.P. Palaio, R.J. Stover, M. Wei, *IEEE Trans. Electron Dev.* 50 (1) (2003) 225–238.
- [18] B. Flaugher, H.T. Diehl, K. Honscheid, et al., *Astr. Journal* 150 (5) (2015) 150, also at arXiv:1504.02900.
- [19] J. Estrada, R. Alvarez, T. Abbott, J. Annis, M. Bonati, E. Buckley-Geer, J. Campa, H. Cease, S. Chappa, D. DePoy, G. Derylo, H.T. Diehl, B. Flaugher, J. Hao, S. Holland, D. Huffman, I. Karliner, D. Kubik, S. Kuhlmann, K. Kuk, H. Lin, N. Roe, V. Scarpine, R. Schmidt, K. Schultz, T. Shaw, V. Simaitis, H. Spinka, W. Stuermer, D. Tucker, A. Walker, W. Wester, *Proc. SPIE* 7735, Ground-based and Airborne Instrumentation for Astronomy III, 2010, 77351R; doi:10.1117/12.857651.
- [20] The DAMIC Collaboration, Measurement of radioactive contamination in the high-resistivity silicon ccds of the damic experiment, *JINST* 10 (2015) P08014.
- [21] J. Estrada, J. Molina, J.J. Blostein, G. Fernandez, *Nucl. Instrum. Methods A* 665 (2011) 90.
- [22] J.J. Blostaina, J. Estrada, A. Tartaglione, M. Sofo Haro, G.F. Moronid, G. Cancelo, *J. Instrum.* 10 (2015) P01006.
- [23] A. Saunders, M. Makela, et al., *Rev. Sci. Instrum.* 84 (2013) 013304.
- [24] Z. Ahmed, et al., arXiv:1803.11306, 2018.
- [25] P. Brax, G. Pignol, D. Roulier, *Phys. Rev. D* 88 (2013) 083004.